Velocity and angular distributions of evaporation residues from ^{32}S-induced reactions

J. D. Hinnefeld* and J. J. Kolata
Department of Physics, University of Notre Dame, Notre Dame, Indiana 46556

D. J. Henderson, R. V. F. Janssens, D. G. Kovar, K. T. Lesko,† G. Rosner,‡
G. S. F. Stephans,§ A. M. van den Berg,** and B. D. Wilkins
Physics Division, Argonne National Laboratory, Argonne, Illinois 60439

F. W. Prosser and S. V. Reinert
Department of Physics, University of Kansas, Lawrence, Kansas 66045

P. L. Gonthier
Department of Physics, Hope College, Holland, Michigan 49423
(Received 26 May 1987)

Velocity distributions of mass-resolved evaporation residues from reactions of ^{32}S with ^{12}C, ^{24}Mg, ^{27}Al, ^{28}Si, and ^{40}Ca have been measured at bombarding energies of 194, 239, and 278 MeV using time-of-flight techniques. In all cases, the observed shifts in the velocity centroids relative to the values expected for complete fusion are consistent with a previously reported parametrization of a threshold for onset of incomplete fusion. Angular distributions were measured and total cross sections extracted for the ^{32}S+^{24}Mg system at all three energies. A comparison with existing results for ^{32}S+^{24}Mg at lower energies, and with other systems leading to the ^{56}Ni compound nucleus, suggests two different types of compound-nuclear limitations to complete fusion at higher energies.

I. INTRODUCTION

Recent investigations of incomplete fusion processes in heavy ion induced reactions suggest a dependence on the degree of mass asymmetry in the entrance channel.[1–3] In particular, velocity measurements[4] of evaporation residues (ER) from ^{16}O+^{40}Ca at energies above 8.5 MeV/nucleon reveal shifts in the centroids of the velocity distributions toward lower values than would be expected for complete fusion, indicating the presence of contributions from incomplete fusion to the evaporation residue yields. Similar measurements on the ^{28}Si+^{28}Si system at comparable compound-nucleus excitation energies,[5] however, show no clear evidence of incomplete fusion. In addition, measured cross sections for ^{28}Si+^{28}Si at the higher bombarding energies ($E_{\rm lab} > 9$ MeV/nucleon) are found to be significantly smaller than observed for ^{16}O+^{40}Ca at comparable energies.[5,6]

The present experiment was performed to explore further the dependence of the incomplete fusion process on the entrance channel by investigating reactions of ^{32}S beams on several targets. Among the systems studied was ^{32}S+^{24}Mg, which leads to the same compound nucleus (^{56}Ni) as the reactions discussed above. Comparison of the ^{32}S+^{24}Mg ER cross sections with those measured previously for ^{16}O+^{40}Ca and ^{28}Si+^{28}Si should provide useful information regarding the mass-asymmetry dependence of the limitations to fusion observed at higher energies.

II. EXPERIMENTAL METHOD AND DATA ANALYSIS

The experiment was performed at the Tandem-Linac accelerator facility at Argonne National Laboratory. Beams of ^{32}S ions at energies of 194, 239, and 278 MeV were incident on targets near the entrance to a 165-cm diameter scattering chamber, and reaction products were detected in a time-of-flight arm consisting of two microchannel plate detectors, separated by about 1 m, followed by a 200 μm thick silicon surface barrier detector. A second silicon detector, 5 mm thick, was used to measure the energy of fast, light ions that were not stopped in the 200 μm detector. The target materials and thicknesses are listed in Table I. The placement of the target near the entrance to the chamber maximized the flight path of the detected reaction products. The separation between the channel plate detector foils varied from 109.72 cm at a detection angle of 2° to 102.04 cm at 20°. Two time measurements were made for each event. Start signals were provided by the back channel-plate detector and the 200 μm silicon detector, and the stop signal for both measurements was provided by a delayed signal from the front channel-plate detector. Mass identification was obtained by using the energy deposited in the Si detector stack and the time of flight from the channel plate–silicon detector (CP-Si) measurement. A typical mass versus velocity plot is shown in Fig. 1(a). The resolution of the CP-Si time measurement was approximately 150 psec FWHM, and the energy resolution

TABLE I. Target materials and thicknesses.

Target material	Isotopic purity	Thickness ($\mu g/cm^2$)
^{12}C	natural	41
^{24}Mg	99.9%	245
^{24}Mg	99.9%	720
^{27}Al	natural	430
^{28}Si	99.4%	125
^{40}Ca	99.9%	315

of the silicon detector was approximately 1.5% at evaporation-residue energies. This provided mass separation for product masses up to about $A=50$, as illustrated in Fig. 1(b).

Elastic scattering and evaporation-residue angular distributions were measured for the $^{32}S+^{24}Mg$ system over the angular range 2° to 20°, in steps ranging from 0.5° at forward angles to 4° at the largest angles. The beam direction was established to within 0.03° from left-right measurements of the elastic scattering at forward angles. Two silicon surface-barrier detectors were used to monitor the $^{32}S+^{24}Mg$ elastic scattering yield during the experiment. Both the monitors and the integrated beam current were used to obtain the relative normalization of the measured differential cross sections. The absolute normalization was obtained by establishing the Rutherford cross section behavior in the elastic scattering at forward angles. The optical-model fits to the measured elastic scattering angular distributions were obtained using PTOLEMY,[7] as shown in Fig. 2. The fit parameters obtained are given in Table II.

For all reactions, measurements of the ER velocity distributions were made at a single angle (6° at $E_{lab}=194$ and 239 MeV and 5° at $E_{lab}=278$ MeV). The velocity spectra of the reaction products were obtained from the channel plate–channel plate (CP-CP) time measurement. The CP-Si timing was not used for the velocity measurement, even though it provided slightly better resolution than the CP-CP timing, because of plasma delay effects.[8] A detailed calibration of the time-to-amplitude converter (TAC) used for the CP-CP time measurement revealed evidence of nonlinearities of the order of 0.5%, for which corrections were made on an event-by-event basis before the calculation of the velocity. The identified masses were used in energy loss calculations to estimate the amount of energy lost by each detected product in the target and the first channel plate detector, in order

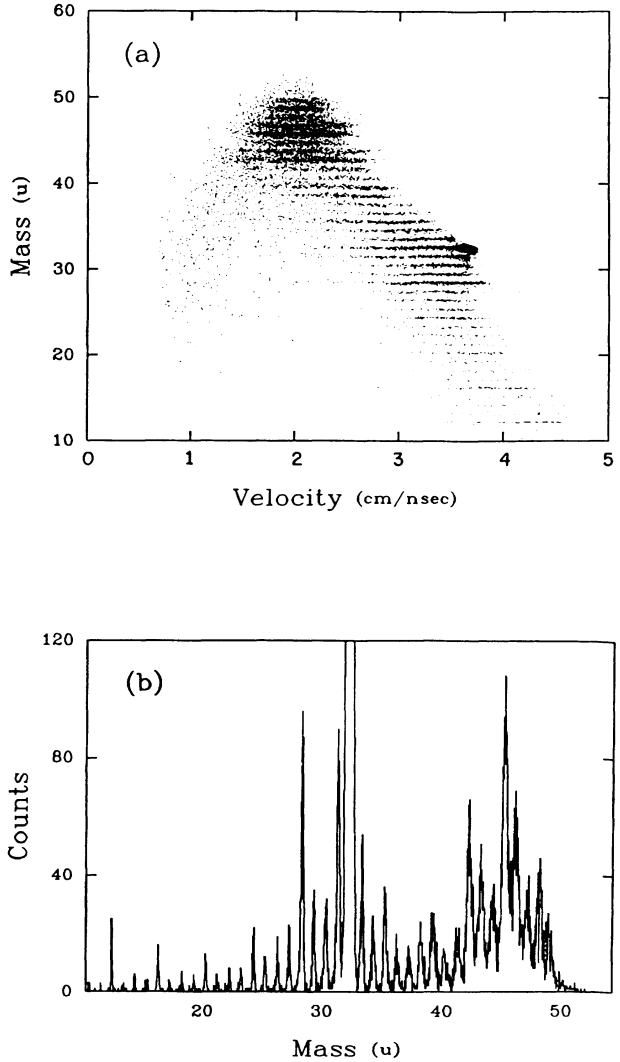

FIG. 1. (a) Two-dimensional plot of mass vs velocity for reaction products from $^{32}S+^{24}Mg$ at $E_{lab}=194$ MeV, detected in the time-of-flight arm at 10°. (b) Projection of (a) onto the mass axis.

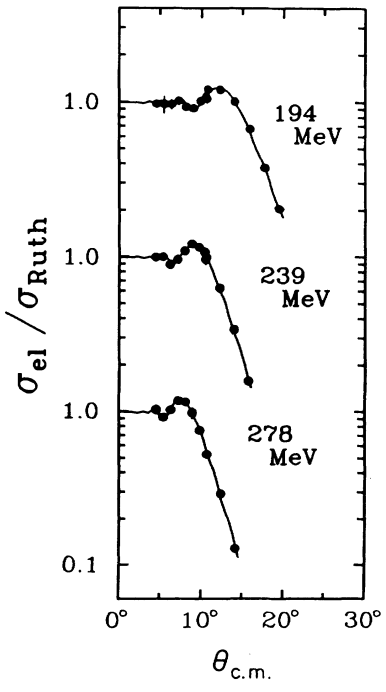

FIG. 2. Elastic scattering angular distributions for $^{32}S+^{24}Mg$, used for absolute normalization of the evaporation residue cross sections. The curves are optical model fits obtained with PTOLEMY using the parameters of Table II.

TABLE II. Elastic scattering optical model fit parameters. Only the well depths, V_R and V_I, were allowed to vary during the fit.

E_{lab} (MeV)	V_R (MeV)	V_I (MeV)	r_{0R} (fm)	r_{0I} (fm)	a_R (fm)	a_I (fm)
194	50.0	38.8	1.22	1.19	0.55	0.55
239	58.8	67.9	1.22	1.19	0.55	0.55
278	46.3	63.0	1.22	1.19	0.55	0.55

to determine its velocity at formation, which was assumed to occur at the target center.

As pointed out previously in the literature,[9] the assumptions of complete fusion and isotropic center-of-mass angular distributions for evaporated light particles imply that the quantity $V_{lab}^{-2}d^2\sigma/d\Omega_{lab}dV_{lab}$ (where V_{lab} is the laboratory velocity of the evaporation residue) should have the form of a Gaussian distribution centered at the velocity $V_{c.m.}\cos\theta_{lab}$ (where $V_{c.m.}$ is the center-of-mass velocity of the projectile-target system and θ_{lab} is the laboratory detection angle). This prediction is in agreement with the results of more detailed Monte Carlo simulations using LILITA.[10] A shift in the centroid of a measured velocity distribution away from this predicted value was taken as evidence that some fraction of the evaporation-residue yield arises from incomplete fusion.

For systems such as those investigated here, in which the compound nucleus mass is not too much different from the projectile mass, there can be some overlap in mass between evaporation residues and products of deep-inelastic (DI) binary reactions. This overlap can lead to some ambiguity in the identification of the evaporation residues. In the case of the $^{32}S+^{40}Ca$ experiment, the ER's were well separated from other reaction products and no ambiguities arose. For the systems $^{32}S+^{24}Mg$, ^{27}Al, and ^{28}Si, however, a mass-by-mass comparison of the measured velocity spectra with the predictions of LILITA revealed a dramatic change in the character of the measured distributions over a span of only one or two masses. This behavior, shown in Figs. 3 and 4 for $E_{lab}=194$ MeV, is observed at all three bombarding energies. Residues with masses greater than those at which this change occurs have been included in composite velocity spectra for each target-energy combination, under the assumption that the data for these residues are not significantly contaminated by contributions due to DI reaction products. Centroids were extracted from these composite spectra by fitting them to Gaussian shapes. As a check on the possible errors inherent in establishing which masses to consider as evaporation residues, the mass cuts were changed by two units in either direction. The resulting changes in the extracted centroids were well within the experimental uncertainties in all cases.

In the case of the $^{32}S+^{12}C$ system there is a more significant overlap in mass, with evaporation residues ex-

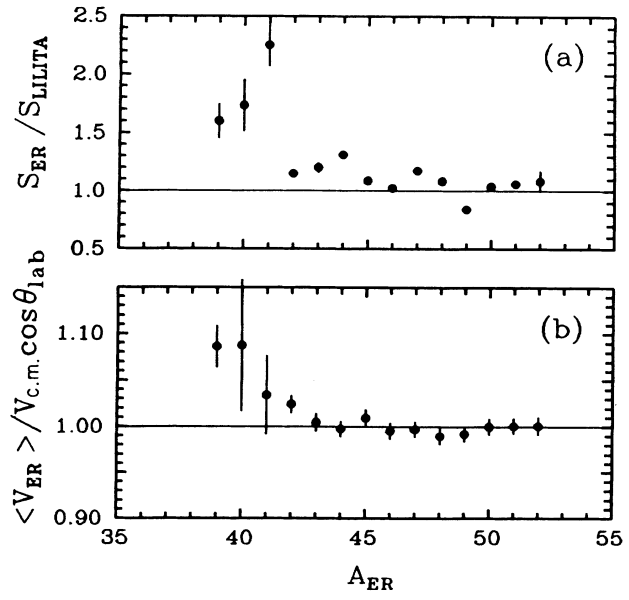

FIG. 3. Comparison of measured (a) widths (FWHM) and (b) centroids of velocity spectra of individual product masses from $^{32}S+^{24}Mg$ at $E_{lab}=194$ MeV with the values expected in the case of complete fusion.

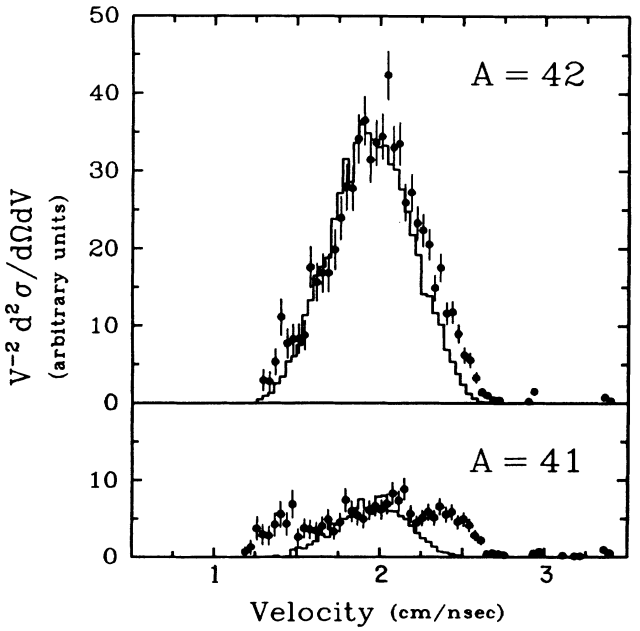

FIG. 4. Velocity spectra of $A=42$ and $A=41$ reaction products from $^{32}S+^{24}Mg$ at $E_{lab}=194$ MeV, showing the dramatic change from a predominance of evaporation residues at $A=42$ to significant low- and high-velocity contributions from binary processes at $A=41$. The histogram is the velocity distribution predicted by LILITA.

tending to masses below that of the projectile. However, there is a rather clear separation in the velocity spectra of individual masses between ER's and products of direct reactions, allowing the extraction of reliable values for the ER velocity centroids. A typical example is shown in Fig. 5. The exclusion of various combinations of masses from the composite spectra produces only very small changes in the centroids, well within the experimental uncertainties at all energies.

The ambiguity in the identification of evaporation residues constitutes the largest uncertainty in the determination of cross sections in the intermediate mass range, especially at larger angles. At angles less than about 10° it is still possible to make a separation based on mass alone, and a reasonable estimate of the ER cross section can be obtained by extrapolating the angular distribution exponentially from that point outward. A more accurate determination can be made, however, from an examination of the velocity spectra of individual reaction products in the overlap region. For each angle in the measured angular distributions, the measured velocity spectra of all product masses, from the highest detected down to those which show no significant contribution from fusionlike processes (typically 15–20 masses per angle), have been compared with the predictions of LILITA. The heaviest products, which are expected to result entirely from fusion-evaporation, have velocity distributions which are generally in very good agreement with those predicted by LILITA (Fig. 6). On the basis of this agreement, upper and lower limits for evaporation residue yields of product masses of ambiguous origin were estimated by comparing the measured velocity distributions with the corresponding LILITA predictions. An example of such a comparison is shown in Fig. 4. For the upper limit, allowance was made for the possi-

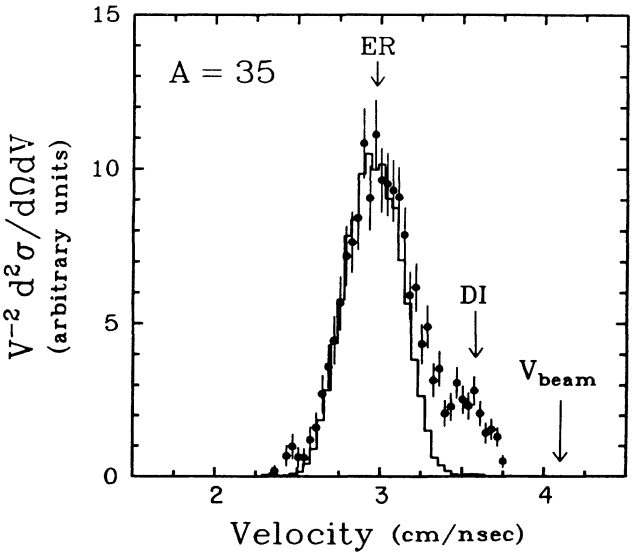

FIG. 5. Velocity spectrum of $A=35$ reaction products from 278 MeV $^{32}S+^{12}C$, detected at $\theta_{lab}=5°$, showing the separation between evaporation residues (ER) and binary, deep-inelastic (DI) reaction products. The histogram represents the ER distribution predicted by LILITA.

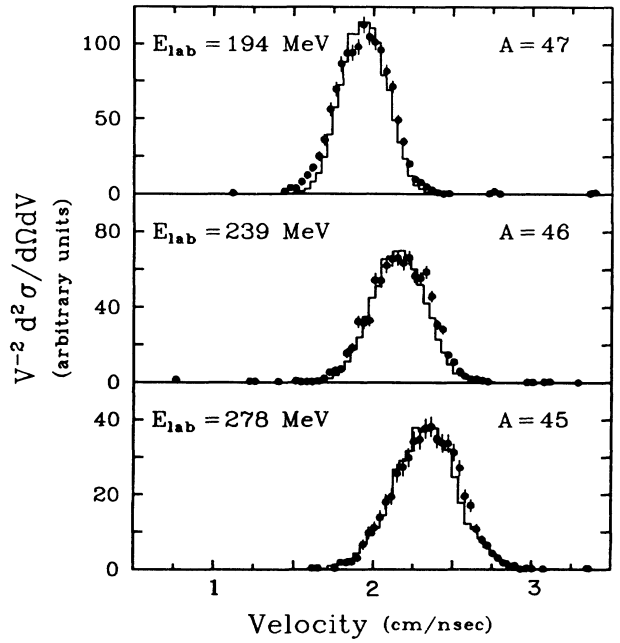

FIG. 6. Velocity spectra of individual mass groups from $^{32}S+^{24}Mg$ reactions, showing good agreement with LILITA calculations (histograms) at the higher residue masses.

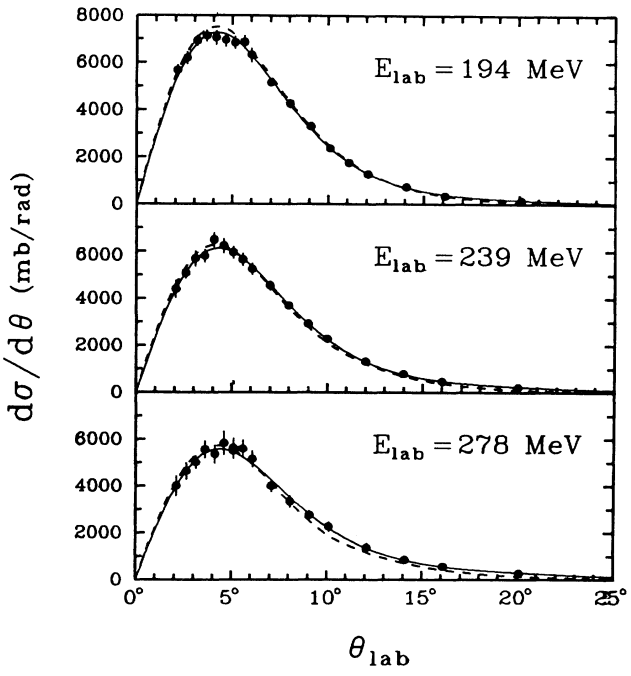

FIG. 7. Measured angular distributions of evaporation residues from $^{32}S+^{24}Mg$ (the error bars reflect uncertainties due to statistics, relative normalizations, and the separation of ER's from other reaction products). The data points shown were obtained from a mass-by-mass comparison with the predictions of LILITA (see text). The solid line is a least-squares fit to these data. The dashed curve was obtained by applying a simple mass cut to the raw data, with an exponential extrapolation to angles beyond $\theta_{lab}=10°$.

bility that the ER velocity distribution might be broadened and slightly shifted by contributions from incomplete fusion processes. Some evidence of a slight broadening and shift was, in fact, observed. However, the effect was small, and as will be discussed later, it is not possible to conclude that evidence for incomplete fusion was observed for the $^{32}S+^{24}Mg$ reaction.

The uncertainty introduced into the ER yield by the procedure outlined above was treated as a systematic error. This accounted for the largest contribution to the overall uncertainty in the measured cross sections (3.5% at 194 MeV and up to 7% at 278 MeV). Other contributions to the uncertainties were due to counting statistics (1–2 %), extrapolation to large angles (1.5–3 %), relative normalizations (1–2%), and absolute normalization (5–8 %). Figure 7 compares the angular distributions obtained by this procedure with those obtained using a simple mass cut and exponential extrapolation.

III. RESULTS AND DISCUSSION

The results of the velocity centroid measurements are plotted in Fig. 8(a) against $V_{\rm rel}$, the relative velocity of the projectile and target at the Coulomb barrier. Morgenstern *et al.*[1] have pointed out that the velocity of the lighter partner in the center of mass frame, V_L, may be related to the onset of incomplete fusion. In Fig. 8(b) the ratio of the measured centroid, $\langle V_{\rm ER}\rangle$, to that expected in the case of complete fusion is plotted as a function of V_L, which is given by

$$V_L=\frac{A_H}{A_H+A_L}V_{\rm rel}\ , \tag{1}$$

where

$$V_{\rm rel}=\sqrt{2(E_{\rm c.m.}-V_{\rm Coul})/\mu}\ . \tag{2}$$

Here A_H and A_L represent the masses of the heavier and lighter reaction partners, respectively, $V_{\rm Coul}$ and $E_{\rm c.m.}$ are the Coulomb and center-of-mass kinetic energies, and μ is the reduced mass of the projectile-target system. With the possible exception of the $^{32}S+^{40}Ca$ system, all the data in Fig. 8 are consistent with a threshold of $V_L\approx 0.06c$ for the onset of incomplete fusion, in agreement with Ref. 1. It should be noted, however, that except for the $^{32}S+^{12}C$ system the values of V_L barely exceed the threshold even at the highest beam energy measured. If the important variable is V_L rather than $V_{\rm rel}$, then the requirement of higher center-of-mass energies is inherent in searches for velocity shifts in nearly symmetric systems. Even for the highly asymmetric $^{32}S+^{12}C$ system, for which V_L approaches $0.09c$, the centroid shift is very small in comparison with previously measured shifts for systems of comparable asymmetry. For example, $^{16}O+^{40}Ca$ at $V_L=0.084c$ exhibits a centroid shift of 6%,[4] and $^{14}N+^{40}Ca$ at $V_L=0.089c$ a shift of 8%,[2] compared with a shift of only 2% for $^{32}S+^{12}C$ at $V_L=0.087c$. This reflects the fact that velocity-measurement experiments using the heavier reaction partner as projectile are made in the rest frame of the lighter partner, in which the center-of-mass velocity (and hence the typical ER velocity, which is approximately equal to $V_{\rm c.m.}\cos\theta_{\rm lab}$) is higher than if the roles were reversed. Therefore, while the *absolute* ER velocity shift associated with an incomplete fusion event is independent of whether the projectile is heavier or lighter than the target, the *relative* velocity shift, i.e., the ratio $\langle V_{\rm ER}\rangle/V_{\rm c.m.}\cos\theta_{\rm lab}$, is smaller by the factor A_L/A_H when the projectile is heavier than the target.

Stephans *et al.*[2] have proposed a model, based on the coupling of the velocities of the colliding nuclei with the intrinsic Fermi motion of the component nucleons, which accounts for some aspects of the onset of incomplete fusion in asymmetric systems. In particular, the

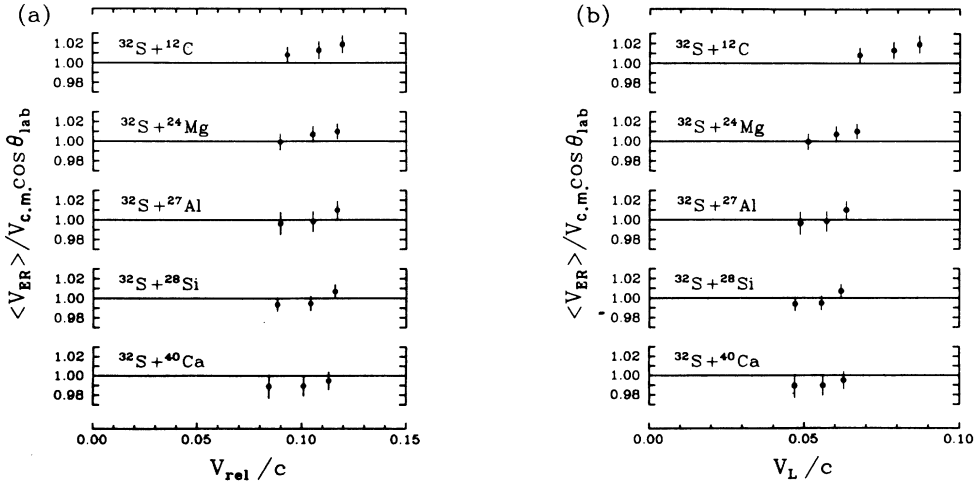

FIG. 8. Ratios of measured velocity centroids of composite spectra to those expected in the case of complete fusion, plotted vs (a) the relative velocity at the Coulomb barrier and (b) the center-of-mass velocity of the lighter reaction partner. The error bars reflect uncertainties due to statistics, the fitting process, the resolution of the time measurements, the energy loss calculations, and the uncertainty in the beam energy.

observed dependence on V_L rather than V_{rel}, and the existence of a threshold value of V_L for the onset of observable velocity shifts, are successfully reproduced. In this model the velocity of each reaction partner relative to the center of mass is added to its distribution of intrinsic nucleon velocities, which is taken to be that of a Fermi gas. The portion of the resultant spherical distribution of velocities which lies outside the corresponding sphere for the fused compound nucleus is then taken as a measure of the average number of nucleons emitted prior to fusion. This quantity can be related to the measured velocity of the fused system by conservation of momentum, under the assumption that the emitted mass acts as a spectator, via the expression

$$A_P V_P = (A_P + A_T - M_P - M_T) V_{RCN} + M_P V'_P + M_T V'_T \ , \tag{3}$$

where A_P and A_T are the masses of the projectile and target, M_P and M_T are the masses of the fragments emitted by the projectile and target prior to fusion, V_P is the beam velocity, and V_{RCN} is the recoil velocity of the "reduced" compound nucleus. The velocity, V'_P or V'_T, of each nonfusing fragment is taken to be the velocity of the reaction partner from which it is emitted, measured at the point of contact:

$$V'_P = V_{c.m.} + V_{rel} \frac{A_T}{A_P + A_T} \ ,$$
$$V'_T = V_{c.m.} - V_{rel} \frac{A_P}{A_P + A_T} \ . \tag{4}$$

Of the five systems for which velocity shifts have been measured in the present experiment, only the $^{32}S + ^{12}C$ system reaches values of V_L that are high enough to allow a meaningful comparison with the predictions of this model. Such a comparison is made in Fig. 9, where the short-dashed lines represent the results of model calculations assuming mass loss from the target only (curving upward) or the projectile only (curving downward) and the long-dashed line includes the effects of mass loss from both the projectile and the target. Values for the Fermi velocities, listed in Table III, were obtained from electron scattering data.[11] The calculation presented in Fig. 9(a) was performed using a compound nucleus Fermi velocity obtained in the same way, while a larger value (Table III) was used for the calculation of Fig. 9(b). It is interesting to note that, while the compound nucleus Fermi velocity has a sizeable effect on the calculations allowing mass loss from only one reaction partner, it has very little effect when mass loss from both partners is allowed. In particular, the threshold for observable velocity shifts is essentially independent of small variations in the CN Fermi velocity when mass loss from both nuclei is allowed.

TABLE III. Fermi velocities V_F used in the mass-loss calculations. The values were taken from Ref. 11, either directly (^{12}C) or by interpolation (^{32}S and ^{44}Ti).

Nucleus	V_F/c
^{12}C	0.2373
^{32}S	0.2619
^{44}Ti	0.2700, 0.2800

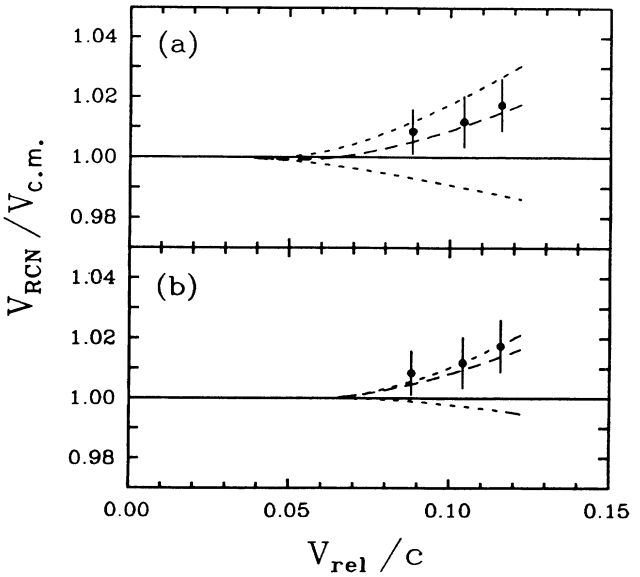

FIG. 9. Comparison of measured velocity centroid shifts with the results of calculations based on the model of Ref. 2. The short-dashed lines correspond to mass loss from the target only (curving upward) or the projectile only (curving downward). The long-dashed line results from allowing mass loss from both. The compound-nucleus Fermi velocities used were 0.2700c for (a) and 0.2800c for (b).

Another aspect of these calculations worth noting is the fact that, depending on the value chosen for the CN Fermi velocity, the predicted average mass loss from the heavier partner is comparable to or even greater than that from the lighter partner even for the asymmetric $^{32}S + ^{12}C$ system. For example, with the smaller CN Fermi velocity used in the calculation of Fig. 9(a) the predicted mass loss from ^{32}S at $E_{lab}(^{32}S) = 280$ MeV is 1.5 u, compared to only 1.3 u from ^{12}C. This illustrates the fact that the observed trends toward lower velocities when the projectile is lighter than the target, and toward higher velocities when it is heavier, do not necessarily imply preferential breakup of the lighter reaction partner. They could simply be a reflection of the fact that a given mass emitted from the lighter reaction partner prior to fusion would tend to take with it a larger fraction of the momentum (in the center-of-mass reference frame) than the same mass emitted from the heavier partner. In light of this observation, and the prediction of comparable mass losses from the projectile and the target, it would be interesting to look for fast, forwardgoing light particles in coincidence with evaporation residues from reactions induced by heavier projectiles on lighter targets. The $^{32}S + ^{12}C$ system might in fact be a good candidate, since such an experiment has already been performed on the system $^{16}O + ^{nat}Ti$, which is very similar in its degree of mass asymmetry, using the lighter nucleus as the projectile.[12]

TABLE IV. $^{32}S+^{24}Mg$ evaporation residue cross sections.

E_{lab} (MeV)	$E_{c.m.}$ (MeV)	σ_{ER} (mb)	σ_{ER}^{CF} (mb)
194	83	1005±65	1005±65
239	102	900±70	855±70
278	119	845±95	790±90

The $^{32}S+^{24}Mg$ evaporation residue cross section measurements are presented in Table IV and plotted along with previous measurements[13,14] in Fig. 10. For purposes of comparison, existing data for $^{28}Si+^{28}Si$ (Refs. 5, 15, and 16) and $^{16}O+^{40}Ca$ (Refs. 6 and 16) are plotted in Fig. 11. The behavior of the $^{32}S+^{24}Mg$ cross section at the higher energies clearly resembles the behavior of the $^{28}Si+^{28}Si$ system more closely than that of $^{16}O+^{40}Ca$. This result, the very slight shifts noted above in the $^{32}S+^{24}Mg$ residue velocity centroids when compared with the much larger shifts measured previously for $^{16}O+^{40}Ca$, and the negligible broadening of the velocity distributions are consistent with an interpretation of the excess $^{16}O+^{40}Ca$ evaporation residue yield as resulting from a larger contribution from incomplete fusion.

The similarity in the behavior of the $^{28}Si+^{28}Si$ and $^{32}S+^{24}Mg$ cross sections is even more evident in Fig. 12, where the excitation energy of the fused compound system (assuming complete fusion) is plotted against the critical angular momentum extracted from the measured cross sections by means of the sharp cutoff approximation. In this approximation, all partial waves with angular momenta below a critical value, l_c, are assumed to lead to fusion with unit probability, and those with larger angular momenta are assumed not to contribute at all to the fusion yield. In this case the fusion cross section can be written as

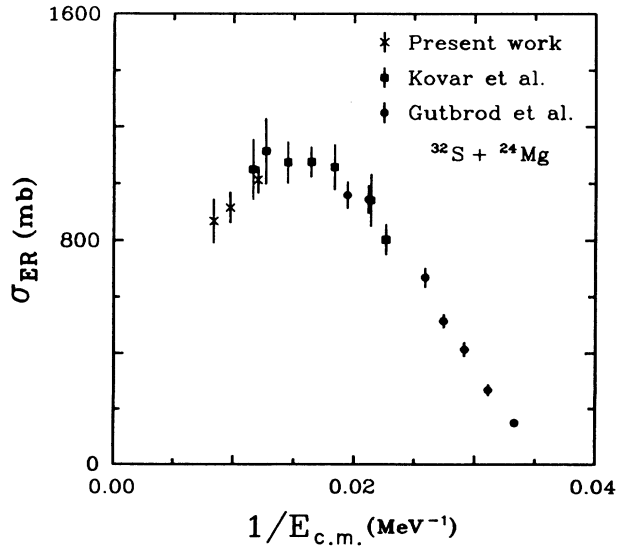

FIG. 10. The total evaporation residue cross sections for $^{32}S+^{24}Mg$ from the present work, along with the existing data from Refs. 13 and 14.

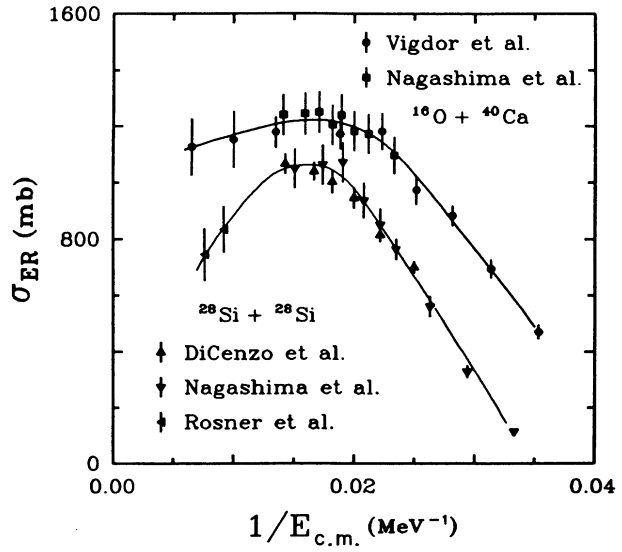

FIG. 11. The total evaporation residue cross sections for $^{16}O+^{40}Ca$ (Refs. 6 and 16) and $^{28}Si+^{28}Si$ (Refs. 5, 15, and 16). The curves are to guide the eye.

$$\sigma_{fus}=\pi\lambda^2\sum_{l=0}^{l_c}(2l+1)\ , \tag{5}$$

where λ is the reduced wavelength of the system. Evaluation of this sum gives

$$\begin{aligned}\sigma_{fus}&=\pi\lambda^2(l_c+1)^2 \quad \text{(distinguishable particles)}\ ,\\ \sigma_{fus}&=\pi\lambda^2(l_c+1)(l_c+2) \quad \text{(identical bosons)}\ .\end{aligned} \tag{6}$$

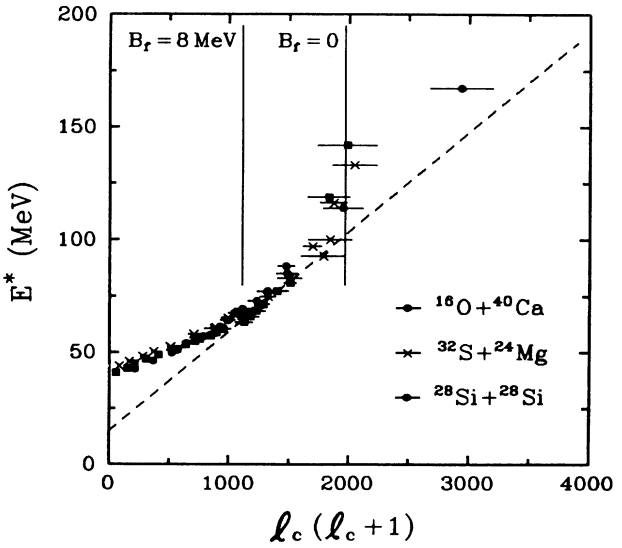

FIG. 12. Compound-nucleus excitation energy vs the product of the critical angular momenta extracted from the ER cross sections in Figs. 10 and 11. The dashed line corresponds to a statistical yrast line (Ref. 17) with parameters $\Delta Q=15$ MeV and $r_0=1.20$ fm. The solid lines indicate the predicted angular momenta for fission barriers of $B_f=0$ and 8 MeV using the model of Sierk (Ref. 20).

Implicit in the application of this description to evaporation residue cross sections is the assumption that the evaporation residues derive only from complete fusion. This may not be a valid assumption at high energies. Nevertheless, if this limitation is kept in mind such plots can be useful in comparing the behavior of different entrance channels leading to the same compound nucleus.

For all three projectile-target systems, division of the E^* versus $l_c(l_c+1)$ plots into three regions with different slopes is suggested, as illustrated schematically in Fig. 13(a). The corresponding divisions in a σ_{ER} versus $1/E_{c.m.}$ plot are shown in Fig. 13(b). These three regions can be associated with three different types of limitations to the fusion cross sections. In region I, where the measured fusion cross section follows very closely the total reaction cross section, numerous studies of light heavy-ion systems have established that the fusion cross section is essentially determined by the ability of the projectile to penetrate the combined Coulomb + centrifugal barrier. In region II the similarity in the E^* versus $l_c(l_c+1)$ plots for all three systems and the linearity of the relationship between E^* and $l_c(l_c+1)$ are suggestive of a limitation related to properties of the ^{56}Ni compound nucleus. Discussions of the mechanism of such a limitation fall into two categories: (1) an entrance channel limitation on fusion imposed by the properties of the compound nucleus,[17,18] or (2) a limitation on the ER cross section imposed by competition in the compound nucleus decay.[19]

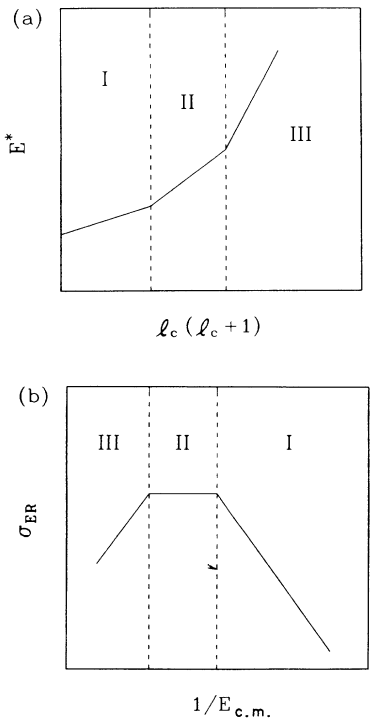

FIG. 13. (a) Schematic diagram illustrating the division of the E^* vs $l_c(l_c+1)$ plot into three regions of different fusion-limiting mechanisms. (b) The corresponding divisions on a plot of σ_{ER} vs $1/E_{c.m.}$.

In the case of an entrance channel limitation, Lee *et al.*[17] have attempted to reproduce the observed cross section behavior for a number of systems using a "statistical" yrast line. The basic assumption underlying this description is that a minimum density of compound-nuclear states is necessary in order for fusion to occur, so that the fusion cross section is limited not by the true yrast line (where the level density is too low for the system to fuse) but by a statistical yrast line which lies at a somewhat higher energy where the level density is higher. The relationship between the excitation energies, E_y^*, and angular momenta, l_y, along this line can be written, under the assumption that it runs parallel to the true yrast line, as

$$E_y^* = \frac{\hbar^2}{2\mathcal{J}} l_y(l_y+1) + \Delta Q \ . \tag{7}$$

Equating the statistical yrast angular momentum, l_y, to the measured critical angular momentum for fusion, l_c, amounts to a parametrization of the fusion limitation in terms of a moment of inertia, $\mathcal{J}$, and energy shift, ΔQ, characteristic of the compound nucleus. This parametrization can be further generalized by the simplifying assumption that the compound nucleus moment of inertia is that of a rigid sphere of radius $R = r_0 A^{1/3}$, so that

$$\mathcal{J} = \tfrac{2}{5} M r_0^2 A^{5/3} \ , \tag{8}$$

where M represents the nucleon mass. If fusion is in fact limited by such a mechanism in region II, the behavior of all three systems should be reasonably well described by a single pair of parameters, r_0 and ΔQ. The dashed line in Fig. 12 corresponds to a statistical yrast line calculated with $r_0 = 1.20$ fm and $\Delta Q = 15$ MeV. The behaviors of all three systems in region II are reproduced rather well by this line.

The similar behavior in region II for the three systems forming ^{56}Ni may also reflect the onset of fission processes which compete with and limit the ER processes. At present our experimental understanding regarding fusion-fission reactions for lighter systems is still unclear. There is evidence from Sanders *et al.*[19] that reaction products consistent with a fusion-fission process are observed beginning at bombarding energies corresponding to region II for ^{16}O+^{40}Ca and ^{32}S+^{24}Mg reactions. The solid lines in Fig. 12 correspond to the angular momenta at which the calculated fission barrier of ^{56}Ni vanishes ($B_f = 0$ MeV) and at which it is approximately equal to the nucleon separation energy ($B_f = 8$ MeV), where one expects fission to begin to become competitive. These calculations use the code of Sierk, which includes the effects of the finite range of the nuclear force and the diffuseness of the nuclear surface.[20] As can be seen in Fig. 12, region II corresponds rather well with the energy range where the fission channel is expected to become increasingly more important. Measurements of the fusion-fission cross sections in this energy range are needed to establish whether the ER behavior is due to competition from the fission channel, an entrance chan-

nel limitation, or a combination of these.

At energies corresponding to regions I and II it is reasonable to assume that the evaporation residue cross section is similar in magnitude to the complete fusion cross section. However, this is not necessarily a valid assumption at region III energies, especially for asymmetric systems. In particular, the two highest-energy $^{16}O+^{40}Ca$ data points in Fig. 12 correspond to energies at which there is clear evidence of contributions to the evaporation residue cross section from incomplete fusion.[4] Therefore these data points have no precise meaning on the plot shown, since the calculations of both a critical angular momentum and a ^{56}Ni excitation energy are predicated on the assumption that the measured cross section corresponds to complete fusion.

The same comments may apply also to the two highest energy $^{32}S+^{24}Mg$ data points, since our ER velocity measurements (see above) do not rule out contributions from incomplete fusion in these cases as well. However, for these two points an estimate can be made of the complete fusion cross section. For each residue mass and at each angle the contribution from complete fusion has been estimated by fitting the velocity spectrum to a multiple-Gaussian distribution, with the centroid and width of one peak fixed by the predictions of the statistical code LILITA. The area of this fixed peak was then taken as an estimate of the complete fusion yield for that mass-angle combination. This is just the procedure referred to in Sec. II for determining the lower limits for the ER yields of individual masses. The resulting complete fusion angular distributions are presented in Fig. 14. The estimated cross sections for complete fusion obtained in this procedure are 855 and 790 mb, at bombarding energies of 239 and 278 MeV, respectively, compared to the cross sections of 900 and 845 mb for ER's (Table IV). A modified version of Fig. 12, with data points extracted only from complete fusion cross sections, is shown in Fig. 15. The uncertainties in the complete fusion differential cross section estimates were taken to be the same as those for the evaporation residue measurements.

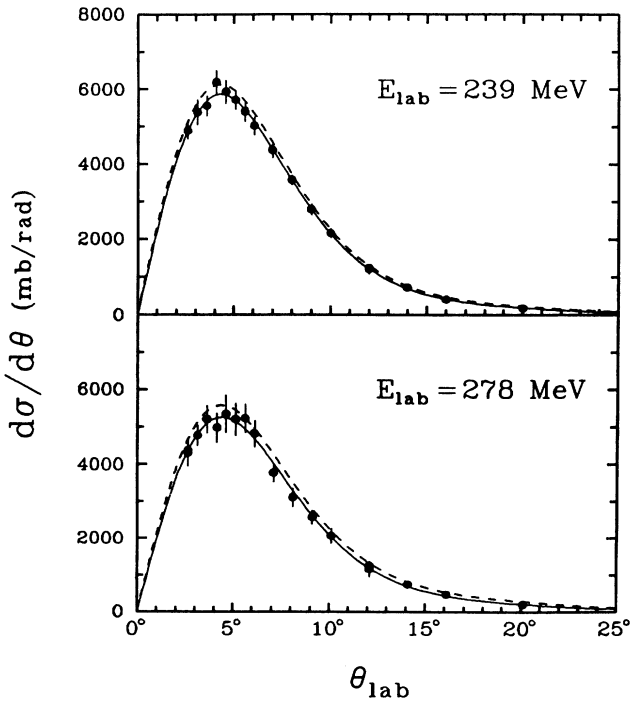

FIG. 14. Complete fusion (data points and solid line) and evaporation residue (dashed line) angular distributions for $^{32}S+^{24}Mg$ at the two highest energies.

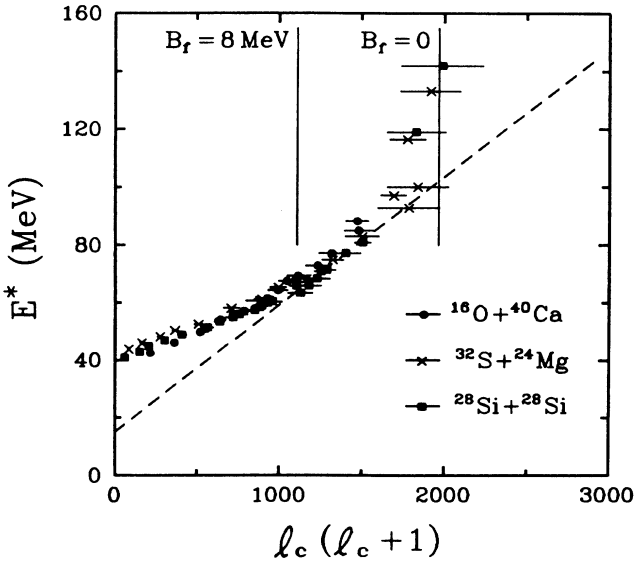

FIG. 15. As in Fig. 12, except that the critical angular momenta are extracted from the estimated complete fusion cross sections.

The mechanism of fusion limitation in region III is less well understood than in the case of regions I and II, although the striking similarity (Fig. 15) between the behaviors of the $^{32}S+^{24}Mg$ and $^{28}Si+^{28}Si$ systems in this region is again strongly suggestive of a limitation based on properties of the compound nucleus rather than the entrance channel. One possibility is that the value of l_c is approaching the limit imposed by the vanishing of the ^{56}Ni fission barrier. A comparison of the data with the Sierk calculations (Fig. 15) shows that the ER cross section behavior is consistent with such an interpretation. Complete fusion estimates for $^{16}O+^{40}Ca$ in region III would be of great interest, since they might determine whether the limitation here is truly independent of the entrance channel. Higher energy measurements for all three systems would also be of interest since it seems likely that an absolute limit to l_c may be reached at excitation energies not much higher than those reported here. Fusion-fission measurements throughout regions II and III would help to untangle the mechanisms involved in the observed limitation to fusion.

IV. SUMMARY

Measurements of the velocity spectra of evaporation residuelike fragments produced in reactions induced by

^{32}S on targets of ^{12}C, ^{24}Mg, ^{27}Al, ^{28}Si, and ^{40}Ca were performed at three bombarding energies over the energy range $6 < E_{lab}(^{32}S) < 8.7$ MeV/nucleon. Clear evidence for incomplete fusion processes was observed in the velocity spectra of the $^{32}S + ^{12}C$ system. For the other systems, there was no conclusive evidence from the centroids of the velocity spectra alone for incomplete fusion contributions

In the case of $^{32}S + ^{24}Mg$, where full angular distributions were also measured, the comparison of the predictions of statistical model calculations to the observed velocity spectra for individual masses suggested small possible incomplete fusion contributions at the higher energies. Based on these comparisons, an estimate of the complete fusion cross section was extracted and found to range between 89% and 100% of the ER cross section at $E_{lab} = 239$ MeV and between 85% and 100% of the ER cross section at $E_{lab} = 278$ MeV. Comparison of these complete fusion cross sections with those measured previously for the $^{28}Si + ^{28}Si$ system at comparable energies indicates a common limitation at compound nucleus excitation energies above about 100 MeV. Coincidence measurements which identify the products of fusion-fission processes are necessary to establish whether the ER cross section behavior is due to the competition of the fission channel, or whether it reflects the complete fusion cross section behavior.

The question of whether the onset of incomplete fusion is different in asymmetric and symmetric entrance channels was not answered in the present study. Inclusive velocity measurements give only limited information, since incomplete fusion contributions broaden rather than shift the velocity distributions of evaporation residues produced in symmetric or nearly symmetric entrance channel reactions. Our comparisons with statistical model calculations were consistent with little or no incomplete fusion contributions in the velocity spectra of evaporation residues produced in the $^{32}S + ^{24}Mg$ reaction up to $E_{lab} = 8.7$ MeV/nucleon, but the possibility of somewhat larger contributions cannot be ruled out. Inclusive measurements at higher bombarding energies to search for an anomalously large broadening, and coincidence measurements of ER fragments with light particles, would provide important information which would shed light on the magnitude of incomplete fusion processes in these systems. For the asymmetric system $^{16}O + ^{40}Ca$ there is clear evidence of incomplete fusion processes at comparable energies from the shifts observed in the velocity spectra. However, ambiguities exist in the identification of evaporation residues and binary reaction products and in the identification of complete and incomplete fusion yields. Coincidence experiments are necessary to resolve these ambiguities. The apparent strong entrance channel dependence of the distribution of reaction strength and of the onset of incomplete fusion processes observed in the symmetric and asymmetric entrance channels forming ^{56}Ni is a very interesting behavior, with implications regarding the fission process in light systems and the mechanism of incomplete fusion processes. Further experiments, most probably coincidence measurements, need to be performed to verify this behavior and to disentangle the various mechanisms.

ACKNOWLEDGMENTS

This work was partially supported by the U.S. National Science Foundation under Grant No. PHY84-16025, and by the U.S. Department of Energy under Contracts DE-AC02-79ER10420 and W-31-109-Eng-38.

---

*Present address: Kernfysisch Versneller Instituut, NL-9747 AA, Groningen, The Netherlands.

†Present address: Lawrence Berkeley Laboratory, Berkeley, CA 94720.

‡Present address: Technische Universität München, Garching, Federal Republic of Germany.

§Present address: Massachusetts Institute of Technology, Cambridge, MA 02139.

**Present address: Rijksuniversiteit Utrecht, The Netherlands.

[1]H. Morgenstern, W. Bohne, W. Galster, K. Grabisch, and A. Kyanowski, Phys. Rev. Lett. **52**, 1104 (1984).

[2]G. S. F. Stephans, D. G. Kovar, R. V. F. Janssens, G. Rosner, H. Ikezoe, B. Wilkins, D. Henderson, K. T. Lesko, J. J. Kolata, C. K. Gelbke, B. V. Jacak, Z. M. Koenig, G. D. Westfall, A. Szanto de Toledo, E. M. Szanto, and P. L. Gonthier, Phys. Lett. **161B**, 60 (1985).

[3]D. G. Kovar, in *Proceedings of the 5th Adriatic International Conference on Nuclear Physics, Croatia, Yugoslavia, 1984*, edited by N. Cindro, W. Greiner, and R. Caplar (World-Scientific, Singapore, 1984), pp. 185–204.

[4]Y. Chan, M. Murphy, R. G. Stokstad, I. Tserruya, S. Wald, and A. Budzanowski, Phys. Rev. C **27**, 447 (1983).

[5]G. Rosner, D. G. Kovar, P. Chowdhury, D. Henderson, H. Ikezoe, R. V. F. Janssens, W. Kuhn, C. S. F. Stephans, B. Wilkins, F. Prosser, Jr., J. Kolata, and J. Hinnefeld, Bull. Am. Phys. Soc. **28**, 670 (1983); G. Rosner, D. G. Kovar, P. Chowdhury, D. Henderson, H. Ikezoe, R. Janssens, W. Kuhn, G. Stephans, B. Wilkins, J. Hinnefeld, J. Kolata, and F. Prosser, Jr., Argonne National Laboratory Physics Division Annual Review, Report ANL-83-25, 1983.

[6]S. E. Vigdor, D. G. Kovar, P. Sperr, J. Mahoney, A. Menchaca-Rocha, C. Olmer, and M. S. Zisman, Phys. Rev. C **20**, 2147 (1979).

[7]M. H. Macfarlane and Steven C. Pieper, Argonne National Laboratory Report ANL-76-11, 1978.

[8]W. Bohne, W. Galster, K. Grabisch, and H. Morgenstern, Nucl. Instrum. Methods Phys. Res. **A240**, 145 (1985).

[9]J. Gomez del Campo, R. G. Stokstad, J. A. Biggerstaff, R. A. Dayras, A.H. Snell, and P. H. Stelson, Phys. Rev. C **19**, 2170 (1979).

[10]J. Gomez del Campo and R. G. Stokstad, Oak Ridge National Laboratory Technical Report ORNL-TM-7295, 1981.
[11]E. J. Moniz, I. Sick, R. R. Whitney, J. R. Ficenec, R. D. Kephart, and W. P. Trower, Phys. Rev. Lett. **26**, 445 (1971).
[12]P. Gonthier, H. Ho, M. N. Namboodiri, L. Adler, J. B. Natowitz, S. Simon, K. Hagel, R. Terry and A. Khodai, Phys. Rev. Lett. **44**, 1387 (1980); H. Ho, P. Gonthier, M. N. Namboodiri, J. B. Natowitz, L. Adler, S. Simon, K. Hagel, R. Terry, and A. Khodai, Phys. Lett. **96B**, 51 (1980).
[13]H. H. Gutbrod, W. G. Winn, and M. Blann, Nucl. Phys. **A213**, 267 (1973).
[14]D. G. Kovar, P. D. Bond, C. Flaum, M. J. Levine, and C. E. Thorn, Bull. Am. Phys. Soc. **22**, 66 (1977); D. Kovar, in Proceedings of the IPCR Symposium on Macroscopic Features of Heavy Ion Collisions and Pre-equilibrium Processes, Hakunc, Japan, 1977, IPCR Cyclotron Progress Report, Suppl. 6, pp. 18–77.
[15]S. B. DiCenzo, J. F. Petersen, and R. R. Betts, Phys. Rev. C **23**, 2561 (1981).
[16]Y. Nagashima, J. Schimizu, T. Nakagawa, Y. Fukuchi, W. Yokota, K. Furuno, M. Yamanouchi, S. M. Lee, N. X. Dai, T. Mikumo, and Y. Motobayashi, Phys. Rev. C **33**, 176 (1986).
[17]S. M. Lee, T. Matsuse, and A. Arima, Phys. Rev. Lett. **45**, 165 (1980).
[18]R. Vandenbosch and A. J. Lazzarini, Phys. Rev. C **23**, 1074 (1981).
[19]S. J. Sanders, R. R. Betts, I. Ahmad, K. T. Lesko, S. Saini, B. D. Wilkins, F. Videbaek, and B. K. Dichter, Phys. Rev. C **34**, 1746 (1986); S. J. Sanders, B. B. Back, R. R. Betts, B. K. Dichter, S. Kaufman, D. G. Kovar, B. Wilkins, and F. Videbaek, in Proceedings of the Symposium on The Many Facets of Heavy-Ion Fusion Reactions, Argonne National Laboratory Report ANL-PHY-86-1, 1986, pp. 219–236.
[20]A. J. Sierk, Phys. Rev. C **33**, 2039 (1986).